Self-Excited Walking of a Biped Mechanism

Kyosuke Ono
Ryutaro Takahashi

Department of Mechanical and Control Engineering
Tokyo Institute of Technology
Tokyo, Japan 152-8552
ono@mech.titech.ac.jp

Toru Shimada

Fujitsu Limited
Kawasaki, Japan

Abstract

The authors studied the self-excited walking of a four-link biped mechanism that possesses an actuated hip joint and passive knee joints with stoppers. They showed that the self-excitation control enables the three-degree-of-freedom planar biped model to walk on level ground by numerical simulation. From the parameter study, it was found that stable walking locomotion is possible over a wide range of feedback gain and link parameter values and that the walking period is almost independent of the feedback gain. Various characteristics of the self-excited walking of a biped mechanism were examined in relation to leg length, and length and mass ratios of the shank. Next, a biped mechanism was manufactured similar to the analytical model. After parameter modification, the authors demonstrated that the biped robot can perform natural dynamic walking on a plane with a 0.8 degree inclination. The simulated results also agree with the experimental walking locomotion.

KEY WORDS—biped mechanism, walking locomotion, self-excitation, natural motion, self-excited walking

1. Introduction

Biped walking is an efficient and sophisticated locomotion that evolved throughout natural history. Few human or bird species attained biped walking. The understanding and development of biped walking robots have been researched since the 1970s. The control methods that have been developed to generate a stable walking gait include the following: the zero moment point (ZMP) method by Kato et al. (1981), the following control of human gait trajectories by Mita et al. (1984), and various kinds of combinations of the model-following control to an inverted pendulum of the support leg and synchronizing control of the swing leg by Miyazaki and Arimoto (1980), Miura and Shimoyama (1984), Furusho and Masubuchi (1986), and Kajita and Kobayashi (1987). Sano and Furusho (1990) paid attention to the model-following control of angular momentum.

On the other hand, McGeer (1990) showed that natural walking of a biped mechanism is possible on an inclined plane using gravitational potential energy. To clarify the fundamental properties of a passive biped system, Goswami, Espiau, and Kermane (1997); Goswami, Thuilot, and Espiau (1998); and Garcia et al. (1998) studied dynamic characteristics of a simple compass-type biped mechanism on an inclined plane as a limit cycle of a nonlinear system including chaos phenomena. Goswami, Espiau, and Kermane (1997) and Spong (1999) investigated active control of the kinetic energy of the biped system to increase the basin of the limit cycle and robustness against disturbance.

Recently, Hirai et al. (1998) developed a sophisticated Honda humanoid biped robot. Since then, humanoid robots with multi-degree-of-freedom (DOF), multifunctional ability, and high adaptability to various circumstances have been developed by several researchers (e.g., Yamaguchi et al. 1998). However, since the Honda robot consumes about 1 kW while walking, it is very important to improve the efficiency of biped walking.

From the aspect of increasing the efficiency of a biped robot, Pratt and Pratt (1998) investigated a control strategy of natural walking motion. As a control method of inducing a natural motion of a passive mechanical system, Ono and Okada (1994a) studied two types of self-excited control: Van der Pol and asymmetrical stiffness matrix. The former was applied to drive an insect wing mechanism (Ono and Okada 1994b), while the latter was applied to drive a rolling motion of a biped mechanism so that it could walk on a level plane by means of the synchronized swing motion of two legs (Ono and Okada 1994c).

The International Journal of Robotics Research
Vol. 20, No. 12, December 2001, pp. 953-966,

This paper describes an investigation of the self-excited walking of a biped mechanism that has a thigh and a shank with a passive knee stopper, creating an efficient natural biped locomotion on level ground. In Section 2, we explain a biped mechanism model and the self-excitation of swing motion of a two-DOF swing leg. In Section 3, the analytical model of a three-DOF biped mechanism and the analytical method are discussed. In Section 4, we show calculated results of stable biped locomotion on level ground and describe various characteristics of the self-excited walking obtained from the simulation study. Then, in Section 5, we explain the manufactured biped robot and experimental results for verification of the theoretical results.

2. Biped Mechanism and Self-Excitation of Swing Leg Motion

2.1. Features of Biped Locomotion and Possibility of Its Self-Excitation

Figure 1 shows a biped mechanism to be treated in this study. Here we focus only on the biped locomotion in the sagittal plane. The biped mechanism does not have an upper body and consists of only two legs that are connected in a series at the hip joint through a motor. Each leg has a thigh and a shank connected at a passive knee joint that has a knee stopper. By the knee stopper, an angle of the knee rotation is restricted like the human knee. The legs have no feet, and the tip of the shank has a small roundness. The objective of this study is to make the biped mechanism perform its inherent natural walking locomotion on level ground not by gravitational force but by active energy through the hip motor.

The necessary conditions for the biped mechanism to be able to walk on level ground are as follows: (1) The inverted pendulum motion of the support leg must synchronize with the swing leg motion. (2) The swing leg should bend so that the tip does not touch the ground. (3) The dissipated energy of the mechanism through collisions at the knee and the ground, as well as friction at joints, should be supplied by the motor. (4) The knee of the support leg should not be bent by the internal force of the knee stopper. (5) The synchronized motion between the inverted pendulum motion of the support leg and the two-DOF pendulum motion of the swing leg, as well as the balance of the input and output energy, should have stable characteristics against small deviations from the synchronized motion.

First we pay attention to the swing leg and try to generate a swing leg motion that can satisfy the necessary conditions (2) and (3) by applying the self-excitation control to the swing leg motion. Ono and Okada (1994a) have already investigated two kinds of self-excitation control of two-DOF vibration systems and showed that the Van der Pol–type self-excitation can evoke natural modes of the original passive system, while the asymmetrical stiffness matrix type can excite the anti-resonance mode that has a phase shift of about 90 degrees between input and output positions.

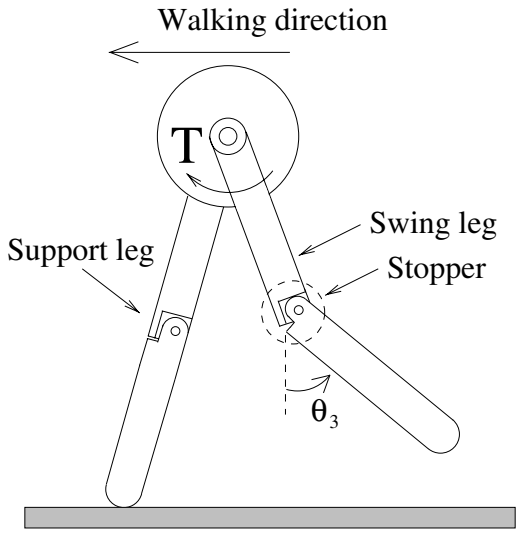

Fig. 1. Three-degree-of-freedom walking mechanism on a sagittal plane.

The two-DOF pendulum of a swing leg has the first-order mode with an in-phase at each joint and the second-order mode with an out-of-phase at each joint. Thus, it will be impossible to generate a walking gait by applying the Van der Pol–type self-excitation. In contrast, by means of the negative feedback from the shank joint angle θ_3 to the input torque T at the thigh joint, the system's stiffness matrix becomes asymmetrical. Thus, the swing motion would change so that the shank motion delays at about 90 degrees from the thigh motion. Through this feedback, it is also expected that the kinetic energy of the swing leg increases and that the reaction torque $(-T)$ will make the support leg rotate in the forward direction in a region where $\theta_3 > 0$. The self-excitation of the swing leg based on the asymmetrical matrix is explained in detail below.

2.2. Self-Excitation of the Swing Leg

Figure 2 depicts the two-DOF swing leg model whose first joint is stationary. To make Figure 2 compatible with Figure 5b, the upper and lower links are termed the second and third links, respectively. To generate a swing motion like a swing leg, only the second joint is driven by the torque T_2, which is given by the negative position feedback of the form

$$T_2 = -k\theta_3. \tag{1}$$

From the fundamental study of the asymmetrical stiffness matrix-type self-excitation (Ono and Okada 1994a), it is known that damping plays an important role in inducing the

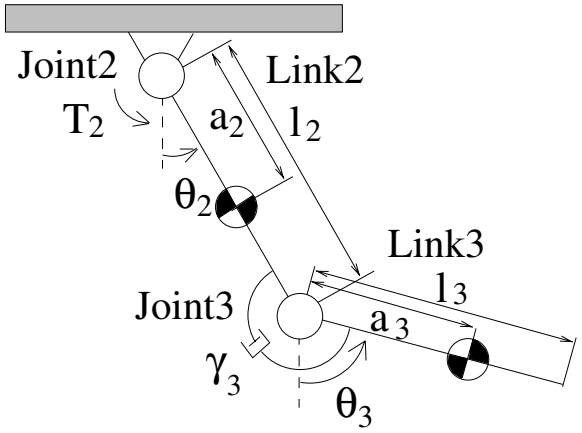

Fig. 2. Analytical model of two-degree-of-freedom swing leg.

self-excited motion. Thus, the viscous rotary damper with coefficient γ_3 is applied to joint 3.

Taking eq. (1) into account, the equation of motion for the two-DOF pendulum system is written as

$$\begin{bmatrix} I_2 + m_2a_2^2 + m_3l_2^2 & m_3a_3l_2\cos(\theta_3-\theta_2) \\ m_3a_3l_2\cos(\theta_3-\theta_2) & I_3 + m_3a_3^2 \end{bmatrix}\begin{bmatrix}\ddot{\theta}_2 \\ \ddot{\theta}_3\end{bmatrix} + \begin{bmatrix} \gamma_3 \\ m_3a_3l_2\sin(\theta_3-\theta_2)\dot{\theta}_2 - \gamma_3 \end{bmatrix} \\ \begin{bmatrix} -m_3a_3l_2\sin(\theta_3-\theta_2)\dot{\theta}_3 - \gamma_3 \\ \gamma_3 \end{bmatrix}\begin{bmatrix}\dot{\theta}_2 \\ \dot{\theta}_3\end{bmatrix} + \begin{bmatrix} (m_2a_2+m_3l_2)g\sin\theta_2/\theta_2 & k \\ 0 & m_3a_3g\sin\theta_3/\theta_3 \end{bmatrix}\begin{bmatrix}\theta_2 \\ \theta_3\end{bmatrix} = 0. \tag{2}$$

We note from eq. (2) that the stiffness matrix of the system becomes asymmetrical because of the feedback gain k.

To examine the value of k to excite a swing leg motion autonomously and the natural frequency and mode at the threshold, eq. (2) is linearized about $\theta_2 = \theta_3 = 0$. The linearized equation of motion becomes

$$\begin{bmatrix} I_2 + m_2a_2^2 + m_3l_2^2 & m_3a_3l_2 \\ m_3a_3l_2 & I_3 + m_3a_3^2 \end{bmatrix}\begin{bmatrix}\ddot{\theta}_2 \\ \ddot{\theta}_3\end{bmatrix} + \begin{bmatrix} \gamma_3 & -\gamma_3 \\ -\gamma_3 & \gamma_3 \end{bmatrix}\begin{bmatrix}\dot{\theta}_2 \\ \dot{\theta}_3\end{bmatrix} + \begin{bmatrix} (m_2a_2+m_3l_2)g & k \\ 0 & m_2a_3g \end{bmatrix}\begin{bmatrix}\theta_2 \\ \theta_3\end{bmatrix} = 0. \tag{3}$$

Putting $\theta_2 = \Theta_2 e^{\lambda t}$ and $\theta_3 = \Theta_3 e^{\lambda t}$ into eq. (3), we have

$$\begin{bmatrix} a_{11}\lambda^2 + \gamma_3\lambda + k_{11} & a_{12}\lambda^2 - \gamma_3\lambda + k \\ a_{21}\lambda^2 - \gamma_3\lambda & a_{22}\lambda^2 + \gamma_3\lambda + k_{22} \end{bmatrix}\begin{bmatrix}\Theta_2 \\ \Theta_3\end{bmatrix} = 0, \tag{4}$$

where $a_{11} = I_2 + m_2a_2^2 + m_3l_2^2$, $a_{12} = a_{21} = m_3a_3l_2$, $a_{22} = I_3 + m_3a_3^2$, $k_{11} = (m_2a_2 + m_3l_2)g$, $k_{22} = m_2a_3g$.

From the condition that the determinant in eq. (4) is zero, we can obtain the characteristic equation of the linearized system of the form

$$A_0\lambda^4 + A_1\lambda^3 + A_2\lambda^2 + A_3\lambda + A_4 = 0. \tag{5}$$

As k increases, one of the eigenvalues becomes unstable. At the boundary, λ becomes an imaginary number. Thus, putting $\lambda = \omega i$ into eq. (5), we can get the critical k value and the natural frequency at the instability threshold.

Here we assume that both links are a uniform bar whose length is 0.4 m ($= l_2 = l_3$), and the mass is 2 kg ($= m_2 = m_3$). For these link parameters, one of the natural modes becomes unstable when $k > 1.43$ or $k < -3.14$. The natural frequency of the unstable swing motion at $k = 1.43$ is 0.71 Hz, whereas that at $k = -3.14$ is 0.61 Hz. If the damping does not exist at joint 3, one of the natural modes becomes unstable when $30.4 > k > 6.3$. Note that the damping coefficient γ_3, however small it might be, can significantly reduce the critical k value. Strangely enough, the magnitude of the damping coefficient γ_3 does not change the critical k value and the natural frequency at the threshold. However, the damping coefficient value slightly influences the natural mode of the unstable vibration. By putting the natural frequency and k value into eq. (4), we found a swing motion such that the lower link delays from the upper link are excited when $k \geq 1.43$. The magnitude and phase of Θ_2/Θ_3 are 0.60 and 8.89 degrees, respectively, when $\gamma_3 = 0.15$ Nms/rad. As the unstable vibration grows in magnitude and approaches a limit cycle, the phase of the Θ_2/Θ_3 tends to be 90 degrees (Ono and Okada 1994a).

2.3. Simulation Results of the Self-Excited Swing Leg

Although the damping enables the system to induce an unstable motion at a small k value as 1.43 within a linear small vibration, it also acts as a damping that limits the amplitude of an unstable motion as the amplitude grows. These effects can be examined by the numerical simulation. For example, a stable limit cycle motion with $\Theta_2 = 0.013$ rad and $\Theta_3 = 0.025$ rad is obtained when the k value is as small as 1.6 Nm/rad and $\gamma_3 = 0.15$ Nms/rad. In such a small amplitude region, the numerically calculated phase delay agrees with the results of the linear analysis. However, when we choose k to be 6.0 Nm/rad, the swing motion grows unlimitedly. Figure 3 shows the time history for the joint angles and stick figures of the swing motion calculated from the nonlinear eq. (2) when $k = 6.0$ Nm/rad and $\gamma_3 = 0.15$ Nms/rad for the same link parameter values as described above. The initial conditions are $\theta_2 = \theta_3 = 0.01$ rad and $\dot{\theta}_2 = \dot{\theta}_3 = 0$. The stick figure shows swing motion from $t = 7.9$ s to $t = 9.0$ s. We note that the swing motion amplitude increases rapidly as time increases and that the amplitude ratio of joint 2 to joint 3 is about 0.4, which is somewhat different from the value of Θ_2/Θ_3 calculated from the linear analysis. We also note that

the phase of joint 3 delays by about 90 degrees from joint 2, so that the swing motion similar to that of the human leg can be realized as seen in the stick figure.

Then, we simulate the swing motion by assuming that joint 3 has a stopper that constrains the motion within the region where $\theta_3 \geq \theta_2$. The collision at the knee is assumed to be completely plastic. After the knee collision, the two-link system behaves as a single-link system if an internal reaction torque exists at the knee. During that time, the asymmetrical feedback is not imposed, so that the link system moves freely. The time history of the joint angles and the stick figures is illustrated in Figure 4. The stick figure represents the swing motion from $t = 7.7$ s to $t = 8.5$ s. We note that a swing motion like a human leg swing can be realized by asymmetrical feedback. Since the exciting force acts only during half the period and the input energy is consumed at the plastic knee collision, the divergence rate becomes small compared with Figure 3.

3. Analytical Model of Biped Locomotion and Basic Equations

The next question is whether the biped mechanism, which combines the two-DOF swing leg discussed in Section 2 and the single-DOF support leg, can generate a biped locomotion that satisfies the conditions (1), (4), and (5). Since it is difficult to derive this solution analytically, we numerically show that the nonlinear biped system excited by the asymmetrical feedback exhibits a stable biped locomotion that satisfies the three conditions as a limit cycle of the system.

Figure 5a shows the representative postures of a biped mechanism during half of the period of biped locomotion. From an aspect of the difference of the basic equation, one step process can be divided into two phases: (1) from the start of the swing leg motion to the collision at the knee (the first phase) and (2) from the knee collision to the touchdown of the straight swing leg (the second phase). We assume that the change of the support leg to the swing leg occurs instantly and that the end of the second phase is the beginning of the first phase. The self-excitation feedback of (1) is applied only during the first phase. We assume that the support leg is kept straight because of internal reaction torque at the knee for simplifying the forward dynamic simulation. The validity of this assumption will be examined later.

Under the assumption of a straight support leg, the analytical model during the first phase is represented as a three-DOF link system, as shown in Figure 5b. Viscous damping is applied to the knee joint of the swing leg. The equation of motion in this system during the first phase is written as

$$\begin{bmatrix} M_{11} & M_{12} & M_{13} \\ & M_{22} & M_{23} \\ sym & & M_{33} \end{bmatrix} \begin{bmatrix} \ddot{\theta}_1 \\ \ddot{\theta}_2 \\ \ddot{\theta}_3 \end{bmatrix} + \begin{bmatrix} 0 & C_{12} & C_{13} \\ -C_{12} & \gamma_3 & C_{23} - \gamma_3 \\ -C_{13} & -C_{23} - \gamma_3 & \gamma_3 \end{bmatrix} \begin{bmatrix} \dot{\theta}_1 \\ \dot{\theta}_2 \\ \dot{\theta}_3 \end{bmatrix} + \begin{bmatrix} K_1 \\ K_2 \\ K_3 \end{bmatrix} = \begin{bmatrix} -T_2 \\ T_2 \\ 0 \end{bmatrix}, \tag{6}$$

where the elements M_{ij}, C_{ij}, and K_i of the matrices are shown in Appendix A. T_2 is the feedback input torque given by eq. (1).

When the shank becomes straight in line with the thigh at the end of the first phase, it is assumed that the knee collision occurs plastically. From the assumption of conservation of momentum and angular momentum before and after the knee collision, angular velocities after the knee collision are calculated from the condition $\dot{\theta}_2^+ = \dot{\theta}_3^+$ and the equation of the form

$$\begin{bmatrix} \dot{\theta}_1^+ \\ \dot{\theta}_2^+ \\ \dot{\theta}_3^+ \end{bmatrix} = [M]^{-1} \begin{bmatrix} f_1(\theta_1, \dot{\theta}_1^-) \\ f_2(\theta_2, \dot{\theta}_2^-) - \tau \\ f_3(\theta_3, \dot{\theta}_3^-) + \tau \end{bmatrix}, \tag{7}$$

where the elements of the matrix $[M]$ are the same as M_{ij} in eq. (6). f_1, f_2, and f_3 are presented in Appendix B. τ is the moment impulse at the knee.

During the second phase, the biped system can be regarded as a two-DOF link system. Thus, the basic equation becomes

$$\begin{bmatrix} I + m_1 a_1^2 + m_2 l_1^2 & m_2 a_2 l_1 \cos(\theta_2 - \theta_1) \\ m_2 a_2 l_1 \cos(\theta_2 - \theta_1) & I_2 + m_2 a_2^2 \end{bmatrix} \begin{bmatrix} \ddot{\theta}_1 \\ \ddot{\theta}_2 \end{bmatrix} + \begin{bmatrix} 0 & -m_2 a_2 l_1 \sin(\theta_2 - \theta_1)\dot{\theta}_2 \\ m_2 a_2 l_1 \sin(\theta_2 - \theta_1)\dot{\theta}_1 & 0 \end{bmatrix} \begin{bmatrix} \dot{\theta}_1 \\ \dot{\theta}_2 \end{bmatrix} + \begin{bmatrix} (m_1 a_1 + m_2 l_1) g \sin\theta_1/\theta_1 & 0 \\ 0 & m_2 a_2 g \sin\theta_2/\theta_2 \end{bmatrix} \begin{bmatrix} \theta_1 \\ \theta_2 \end{bmatrix} = 0. \tag{8}$$

We assume that the collision of the swing leg with the ground occurs plastically (the translational velocity at the tip of the swing leg becomes zero) and that there is a sufficient friction between the tip and the ground surface to prevent slippage. The angular velocities of the links after the collision are derived from conservation laws of momentum and angular momentum. They are calculated from eq. (7) by putting $\tau = 0$.

To investigate the self-excited biped locomotion, a set of basic equations of (6), (7), and (8) were numerically solved based on the fourth-order Runge-Kutta method. The standard values of the link parameters used in the calculation are shown in Table 1. The values of mass and moment of inertia were calculated assuming uniform mass distribution along the link. Since the magnitude of the damping coefficient scarcely influences the biped gait, $\gamma_3 = 0.15$ Nms/rad was used in the calculation.

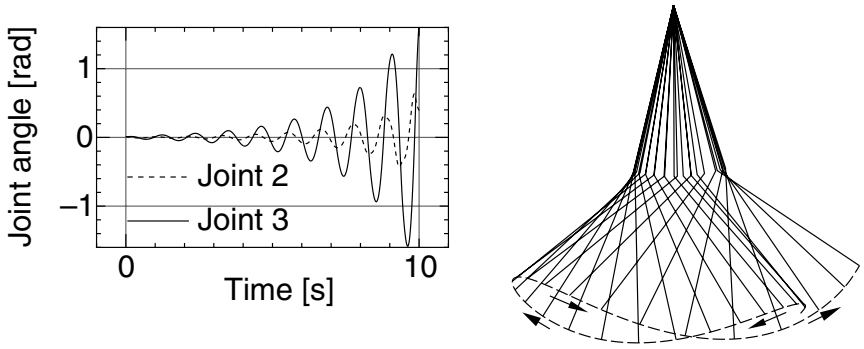

Fig. 3. Self-excited motion of swing leg without knee stopper (initial condition: $\theta_1 = \theta_2 = 0.01$ [rad], $\dot{\theta}_1 = \dot{\theta}_2 = 0$ [rad/s]).

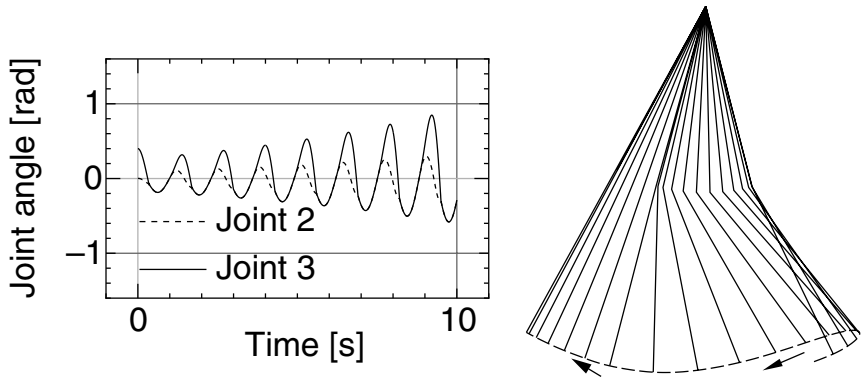

Fig. 4. Self-excited motion of swing leg with knee stopper (initial condition: $\theta_1 = 0.0, \theta_2 = 0.4$ [rad], $\dot{\theta}_1 = \dot{\theta}_2 = 0$ [rad/s]).

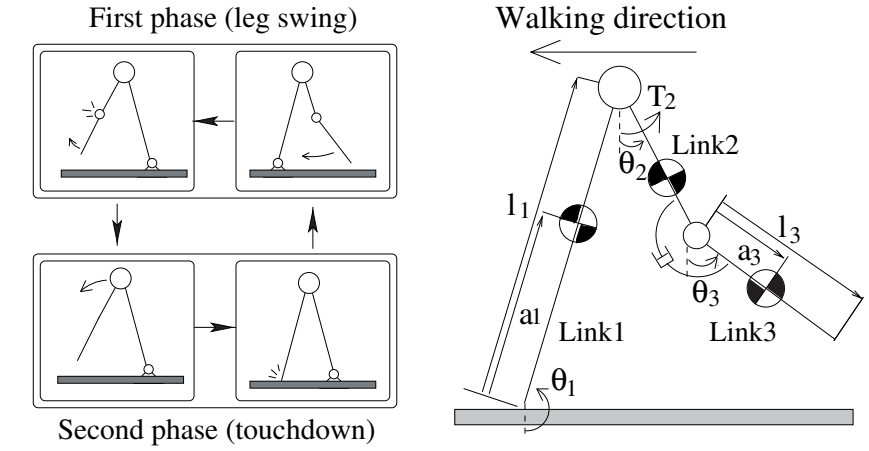

(a) Two phases of biped walking (b) Three-DOF model

Fig. 5. Analytical model of three-degree-of-freedom walking mechanism.

Table 1. Link Parameter Values Used for Simulation Study

	Link 1	Link 2	Link 3
m_i: mass (kg)	4.0	2.0	2.0
l_i: length (m)	0.80	0.40	0.40
I_i: moment of inertia (kgm^2)	0.21	0.027	0.027
a_i: offset of mass center (m)	0.40	0.20	0.20

4. Simulation Results and Characteristics of Self-Excited Walking

4.1. Typical Features of Steady Biped Locomotion

The characteristics of the self-excited biped locomotion are determined by parameter values of the biped mechanism and feedback gain k only. The steady biped locomotion is first presented for the standard parameter values shown in Table 1. The standard feedback gain k is chosen to be 6.0 Nm/rad. Since the steady biped locomotion is a limit cycle motion of the self-excited biped mechanism, the time history calculation of the biped mechanism must start from initial states within the basin of the limit cycle. To guess the initial conditions that lead to a stable limit cycle, at the beginning of the first phase, we modeled the support leg to be a single-DOF inverted pendulum that has the moment of inertia and mass of the support leg at the mass center. The effect of the mass of the swing leg is considered to be added at the hip. From a simple linearized analysis, it is known that the ratio of the initial angular velocity ω_0 and the step angle $2\theta_0$ has a relationship of $\omega_0/\varphi_0 = \lambda_0 \cosh(\lambda_0 T/4)/\sinh(\lambda_0 T/4)$, where $\lambda_0 = \sqrt{m_1(a_1 + l_1)g/I_1}$. Since half of the period T of the swing leg is about 0.65 s, as seen in Figure 4, regardless of the swing amplitude, the support leg with the parameter values shown in Table 1 has a relationship of $\dot{\theta}_1 (= \omega_0) = 7.53 \times \{\theta_0 (= \pi - \theta_1)\}$ at the beginning of the first phase to synchronize the swing leg motion. On the other hand, the swing leg should have initial conditions such as $\theta_2 = \theta_3 = \theta_0$ and $\dot{\theta}_2 = \dot{\theta}_3 = 0$ at the beginning of the first phase. From the simulation using these initial conditions, we found that the same stable limit cycle of biped locomotion with a step length of about 0.18 m can be obtained from any initial value of step length between 0.1 m and 0.25 m. In a parameter study, we also used the initial condition that was on a point of the limit cycle obtained for the previous parameter values.

Figure 6a illustrates the stick figure of the stable self-excited walking gait during two steps (one walking period). The walking period is 1.30 s, and the posture of the biped is illustrated every 0.136 s. We note the shank motion of the swing leg delay from thigh motion so that the swing leg does not hit the ground. The horizontal velocity at the hip is not uniform and decreases to a small value before the support leg passes through the vertical position.

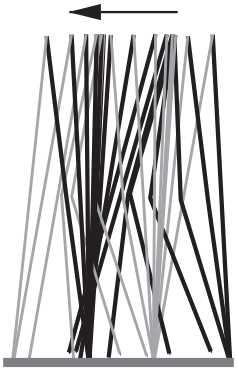

(a)Stick figure of one walking cycle

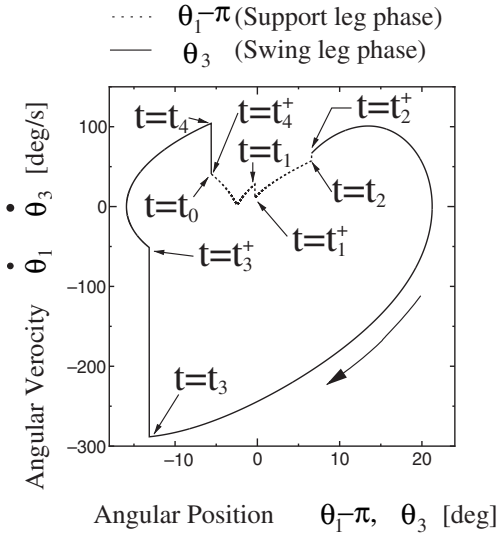

(b)Phase plane illustration of one walking cycle

Fig. 6. Self-excited walking gait and its phase plane illustration ($k = 6.0$ Nm/rad, $T = 1.3$ s).

The change of angular position θ_3 and velocity $\dot{\theta}_3$ of the shank during one period is shown in the phase plane in Figure 6b. During the support phase of the shank from $t = t_0$ to $t = t_2^-$, $\theta_1 - \pi$ and its velocity $\dot{\theta}_1$ are plotted with a dotted line, whereas θ_3 and $\dot{\theta}_3$ during the swing phase are plotted with a solid line. Zero angular position of $\theta_1 - \pi$ and θ_3 means that the shank is in the vertical posture. Strictly speaking, the calculated walking motion is influenced by the time step in the numerical simulation because this system contains collision. When the time step is large, the phase plane trajectory fluctuates at each step, but it converges a unique solution as the time step decreases. In Figures 6a and 6b, the steady limit cycle calculated at the 0.25 ms time step is shown because it can be drawn by one line. In this case, the accuracy of heel height at collision is within 0.05 mm and that of knee angle at collision is within 0.0002 rad (0.69′).

We note from Figures 6a and 6b that the angular velocity of the support leg takes a minimum value close to zero before the support leg passes the vertical position. We also note that the knee collision occurs at $t = t_1$ before the support leg passes the vertical position. At the knee collision, the angular velocity of the support leg decreases slightly. When the tip of the swing leg touches the ground at $t = t_2$, the angular velocity of the support leg increases suddenly. Then the swing motion of the shank begins at $t = t_2^+$. In the beginning of the swing leg motion, $\dot{\theta}_3$ is positive so that θ_3 increases. Then $\dot{\theta}_3$ turns to negative, and θ_3 decreases to a certain negative value until the shank becomes straight with the thigh at $t = t_3$. Due to the knee collision of the swing leg, the angular velocity of the shank changes suddenly from about -290 degrees/s at $t = t_3^-$ to -50 degrees/s at $t = t_3^+$. During the free motion of the biped mechanism in the second phase, $\dot{\theta}_3$ continues to increase from negative to positive values until the tip of the shank hits the ground. At the instant when the straight swing leg touches the ground, the positive angular velocity of the straight swing leg at $t = t_4^-$ drops to the beginning angular velocity of the support leg at $t = t_4^+$. Obviously, the angular velocity of the support leg $\dot{\theta}_1$ should remain positive to maintain a stable biped locomotion.

In this simulation, we assumed that the support leg is kept straight due to internal torque during the first and second phases. To check whether the support leg can be kept straight by the passive knee stopper, the internal torque at the knee of the two-DOF support leg model was inversely calculated by using the calculated stable biped locomotion. Figure 7 plots the angular displacement of $\theta_1 - \pi$, θ_2, and θ_3 and the internal torques at the knees of the support and swing legs, which are calculated from θ_1, θ_2, and θ_3 based on the inverse dynamic analysis. The torque curve at $\phi_{off} = 0 (= \theta_2 - \theta_3)$ indicates the calculated knee torque when the shank is constrained to be such that $\phi_{off} = \theta_2 - \theta_3 \leq 0$. If the knee torque is negative, the reaction torque exists at the knee stopper so that the support leg can be regarded as a single-DOF link. We observe that at the beginning of the first phase, the knee torque of the support leg becomes positive for a short time of less than 0.1 s.

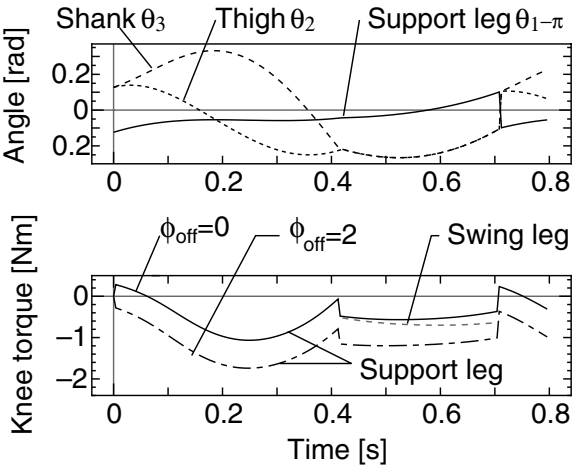

Fig. 7. Motion of legs and internal torque at knee during one step.

Then, we calculated the knee torque of the support leg by assuming an offset angle of $\phi_{off} = \theta_2 - \theta_3 = 2$ degrees at the knee stopper. The calculated result is also shown in Figure 7. We note that the knee torque of the support leg shifts downward and changes to a negative value during the entire period. Moreover, it is seen from the negative knee torque of the swing leg that the swing leg can be kept straight during the second phase.

4.2. Effect of Feedback Gain on Steady Biped Locomotion

All calculated data that will be shown below were obtained by using the time step of 2 ms from a compromise between the calculation accuracy and computing time. In the case of the 2 ms time step, the heel height at collision was distributed within 0.8 mm, and knee angle at collision was distributed within 0.0014 rad. Therefore, the occurrence of heel collision was determined if the heel height was less than 0.4 mm from the floor, while the occurrence of the knee collision was determined if the shank angle relative to the thigh was less than 0.007 rad. We think that this calculation accuracy is practically sufficient because the variations of heel position and knee angle of these levels at the heel and knee collisions will be inevitable in an actual case, even in a controlled experimental condition.

In the numerical simulation, steady biped locomotion can be obtained as a limit cycle for the feedback gain value in a range of 4.8 Nm/rad $\leq k \leq$ 7.5 Nm/rad. When k is smaller than 4.8 Nm/rad, the initial step length gradually decreases and the biped mechanism falls down forward. When k is larger than 7.5 Nm/rad, the step changes irregularly and the biped mechanism falls down backwards because the swing leg is raised too high. Figure 8 shows the walking period, average velocity, and efficiency as a function of feedback gain k. The

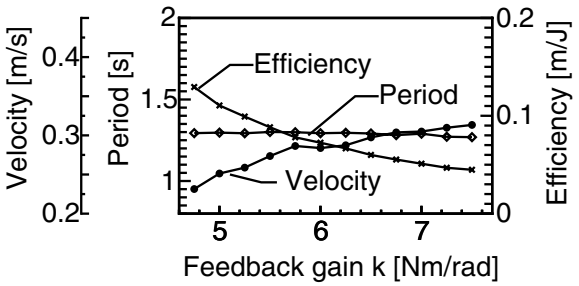

Fig. 8. Effect of feedback gain on walking period, velocity, and efficiency.

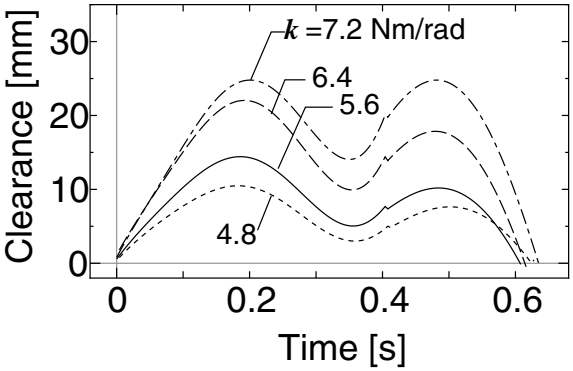

Fig. 9. Effect of feedback gain on swing leg clearance.

efficiency is defined as the ratio of average walking velocity to average input power, where the average input power is given by

$$P = \frac{1}{t_4 - t_0} \int_{t=t_0}^{t=t_4} \left| \dot{\theta}_2 T_2 \right| dt. \tag{9}$$

We note from this figure that the walking period shows an almost constant value of 1.3 s at any k value. This is because the self-excited biped locomotion is a natural motion inherent in the biped system. On the other hand, the average velocity increases gradually because of the increase in step length. However, the efficiency decreases with an increase in the feedback gain k because the average input power increases more rapidly with an increase in k. It is worthy to note that the average input power to generate biped locomotion with a velocity of 0.28 m/s is only about 4 W (= 0.28/0.07) at $k = 6.0$ Nm/rad. If the additional movement of 0.6 m by feet during one period of 1.3 s is taken into account, the natural walking velocity becomes 2.7 km/h. The natural walking period of an adult with a 0.9 m leg height is 1.3 s (Yang 1994). Thus, it can be said that the calculated results of the walking period and velocity are comparable with the natural walking of an adult with a 0.8 m leg height.

Figure 9 shows the height of the tip of the swing leg as a function of time for various values of feedback gain k. We note that the swing leg is lifted higher as the feedback gain increases. From this figure, it is seen that an increase in k causes the increase in swing leg height rather than the increase in step length.

4.3. Effect of Link Parameter Values on Steady Biped Locomotion

It is interesting to examine the effect of link parameter values on walking gait, period, velocity, efficiency, and robustness of stable walking to feedback gain and initial conditions. In particular, optimum link parameter values in terms of walking velocity and efficiency are of our concern. Here we show the steady walking characteristics when total leg length and length and mass ratios of the shank are changed. In the following calculation, the damping coefficient at the knee joint is $\gamma = 0.15$ Nms/rad.

As shown in Figure 8, a stable walking locomotion can be obtained for a wide range of k values. If we choose the middle value of the effective k range, the stable walking locomotion has the most robustness to initial conditions. Thus, the medium of the range is considered to be the optimum value of k for a set of given values of the link parameters. The optimum value and the range of value k that results in a stable biped locomotion change depending on the link parameter values. Therefore, we show the biped locomotion at the optimal k value for a set of link parameter values. A stable biped locomotion can be obtained for the widest range of link parameter values when we choose the optimum k value.

Figure 10 shows the effect of leg length $l_1 (= l_2 + l_3)$ on the walking period, velocity, and efficiency when $m_1 = 4.0$ kg, $m_2 = m_3 = 2.0$ kg. The thigh length (l_2) and shank length (l_3) were changed equally, and the moment of inertia was calculated assuming a uniform mass distribution in both the thigh and shank. Stable walking is obtained when l_1 is no less than 0.5 m, although results when l_1 is larger than 1.8 m are not shown in Figure 10. If $k = 6.0$ Nm/rad is chosen instead of the optimum k value defined above, a stable biped locomotion is possible in a range of $0.6m \leq l_1 (= l_2 + l_3) \leq 0.96$ m. We note from Figure 10 that the walking period and velocity increase with an increase in the leg length because the increasing rate of the step length is larger than that of the period. In addition, the efficiency (velocity/input power) increases with an increase in the leg length. The increasing rate of the efficiency is larger than that of velocity because the average input power decreases slightly with an increase in the leg length. Note that these results are obtained from the assumption that the total mass of leg is constant.

It is commonly known that the mass of the human body is proportional to the square of body length. The walking

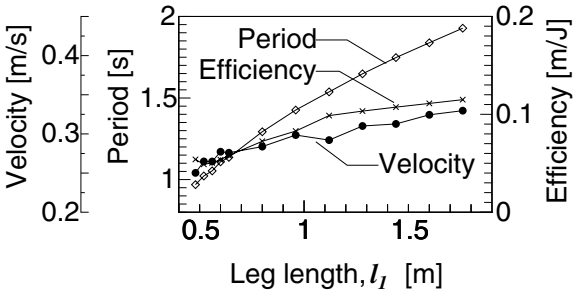

Fig. 10. Effect of leg length on walking characteristics when the leg mass is constant ($l_2 = l_3, m_2 = m_3 = 2$ kg).

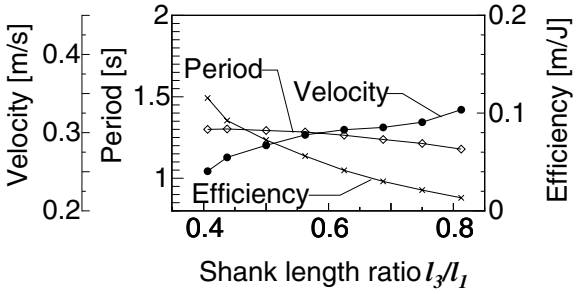

Fig. 12. Effect of shank length ratio on walking characteristics ($l_1 = l_2 + l_3 = 0.8$ m, $m_2 = m_3 = 2$ kg).

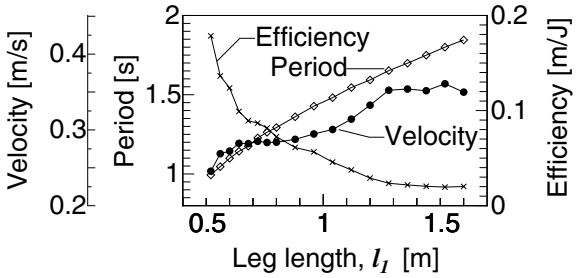

Fig. 11. Effect of leg length on walking characteristics when the leg mass is proportional to square of the leg length ($l_2 = l_3, m_2 = m_3 = 2$ kg at $l_2 = l_3 = 0.4$ m).

characteristics were next calculated under the assumption that the mass of leg increases proportionally to the square of leg length. The calculated results at the optimum k value are shown in Figure 11. The period and velocity increase with an increase in the leg length similar to the constant mass condition shown in Figure 10. However, it is noteworthy that the walking velocity is almost constant in a leg length range of 0.65 m to 0.9 m, which is in the same leg length range of human adults. Contrary to Figure 10, the efficiency decreases monotonically as the leg length increases because the input power increases markedly due to a remarkable increase in the optimum feedback gain. From Figures 10 and 11, it can be said that a person of standard weight with shorter legs is better in terms of efficiency, although he or she may have a slight disadvantage of walking velocity as far as natural walking is concerned. However, if a tall person restricts his or her weight to be the same as that of a short person, he or she will have an advantage in both walking velocity and efficiency.

Although not illustrated here, the period and velocity are not affected by the mass or mass density of the leg but are slightly affected by the moment of inertia or the distribution of mass. In contrast, the input power increases in proportion to the weight of the leg. This may be understood from the slight change of the period and velocity and the big change of the efficiency in Figures 10 and 11.

The effect of the shank length ratio l_3/l_1 on walking characteristics was next examined under the assumption that the total leg length $l_1(= l_2 + l_3)$ is 0.8 m and $m_2 = m_3 = 2$ kg. The center of mass and the moment of inertia of thigh and shank were calculated assuming a uniform mass distribution in the thigh and shank. A stable biped locomotion is possible in a range from $l_3/l_1 = 0.406(l_2 = 0.475$ m, $l_3 = 0.325$ m) to $l_3/l_1 = 0.81(l_2 = 0.15$ m, $l_3 = 0.65$ m) when the optimum k value is chosen for each case. The calculated walking characteristics at the optimum k value are shown as a function of the shank length ratio l_3/l_1 in Figure 12. We note that stable walking is easily obtained when the shank length is longer than the thigh length. The period decreases slightly, but the velocity increases markedly with an increase in l_3/l_1 because of the increase in step length. However, the efficiency decreases as l_3/l_1 increases since the input power markedly increases with an increase in l_3/l_1. Therefore, it can be said that the shank length ratio of about 0.55 in human adults is adequate in terms of both walking velocity and efficiency.

Figures 13a and 13b portray typical stick figures of one walking locomotion cycle when $l_3/l_1 = 0.75(l_2 = 0.2$ m, $l_3 = 0.6$ m) and $l_3/l_1 = 0.44(l_2 = 0.45$ m, $l_3 = 0.35$ m), respectively. We note from these figures that a longer shank can have a larger step length. To show the effect of the shank length ratio on walking gait, the clearance of the tip of the swing leg from the ground is plotted as a function of time in Figure 14. We note that the clearance of the swing leg tip becomes minimum in the middle of the swing phase and that the minimum clearance becomes maximum when the shank length ratio is between 0.5 and 0.62. Since this minimum clearance can be regarded as a margin of stable walking, it can be said that the shank length ratio in standard adults is optimal in terms of stable and robust walking gait.

The effect of shank mass ratio to leg mass m_3/m_1 on walking characteristics was next examined when other parameter values were unchanged. The total mass of the leg $m_1(= m_2 + m_3)$ was kept at 4.0 kg. The center of mass and the moment of inertia of the thigh and shank were calculated

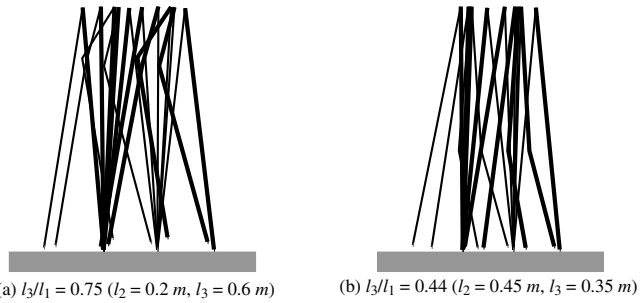

(a) $l_3/l_1 = 0.75$ ($l_2 = 0.2$ *m*, $l_3 = 0.6$ *m*) (b) $l_3/l_1 = 0.44$ ($l_2 = 0.45$ *m*, $l_3 = 0.35$ *m*)

Fig. 13. Stick figure of walking gait for different shank length ratio l_3/l_1 ($l_1 = l_2 + l_3 = 0.8$ m, $m_2 = m_3 = 2$ kg).

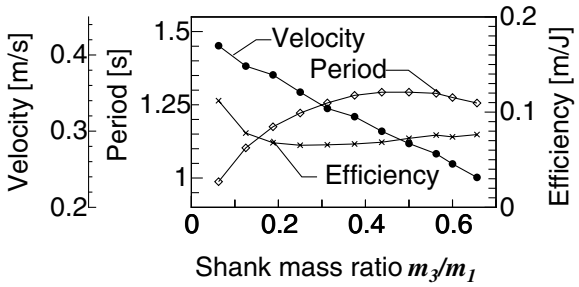

Fig. 15. Effect of shank mass ratio m_3/m_1 on walking characteristics ($m_1 = m_2 + m_3 = 4$ kg, $l_2 = l_3 = 0.4$ m).

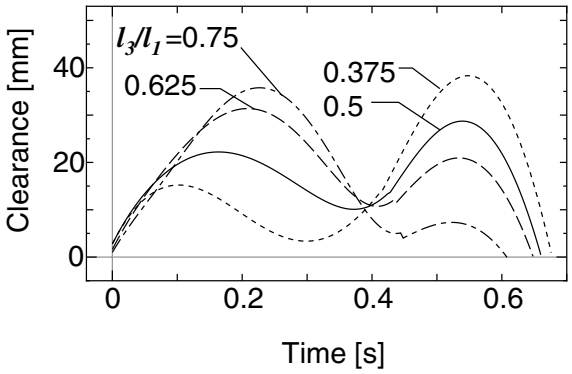

Fig. 14. Effect of shank length ratio l_3/l_1 on swing leg clearance ($l_1 = l_2 + l_3 = 0.8$ m, $m_2 = m_3 = 2$ kg).

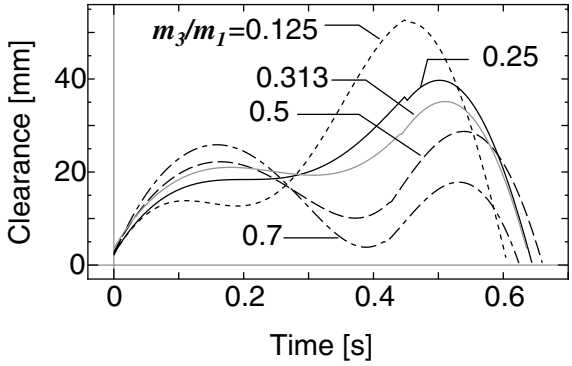

Fig. 16. Effect of shank mass ratio m_3/m_1 on swing leg clearance ($m_1 = m_2 + m_3 = 4$ kg, $l_2 = l_3 = 0.4$ m).

in each case under the assumption of a uniform mass distribution. Figure 15 shows the calculated walking characteristics. We note from this figure that stable walking is possible in a wide range of mass ratios from nearly 0 to 0.7. The walking period is almost maximum when the shank mass ratio is 0.5. The walking velocity increases linearly as the mass ratio decreases. The efficiency is almost constant in a wide range of shank mass ratios but tends to increase as the mass ratio decreases from 0.2. This is because the average input power becomes maximum near the 0.2 mass ratio, although the optimum feedback gain decreases monotonically with a decrease in mass ratio. From these results, it can be said that both the velocity and efficiency increase as the shank mass ratio decreases from 0.2 and that a lighter shank is better in terms of both velocity and efficiency.

The relationship between clearance of the swing leg tip and shank mass ratio is shown in Figure 16. We note that the shank mass ratio value of about 0.3 is optimum in terms of the stable and robust walking gait. From the parameter study described above, it seems that the simulation results are consistent with walking characteristics of a human being.

5. Experimental Study

5.1. Experimental Biped Robot

To validate the simulation results stated above, we manufactured the biped robot similar to the analytical model shown in Figure 5b. The structure of the robot is schematically illustrated in Figure 17. The robot has three legs whose outer legs are connected by a shaft at the hip to prevent a rolling motion. The shaft and the inner leg are connected serially by a 100 W AC servomotor through one-tenth reduction gears. The thigh and shank of each leg are connected by a passive joint with a knee stopper. An optical encoder of 1000 pulses is mounted at each knee joint. To equalize the total mass and moment inertia of each leg, the inner leg is made of an aluminum alloy frame with a 40-by-80 mm cross section, while a couple of the outer legs are made of a 30-by-80 mm frame.

In the self-excitation control, the absolute angle of the shank (θ_3) must be detected. Since the available small gyroscope sensors are too sensitive to impact disturbances at the collision with the ground, the absolute shank angle is estimated from the relative angles measured by the optical encoders at the knee and the hip motor. If the relative angle at

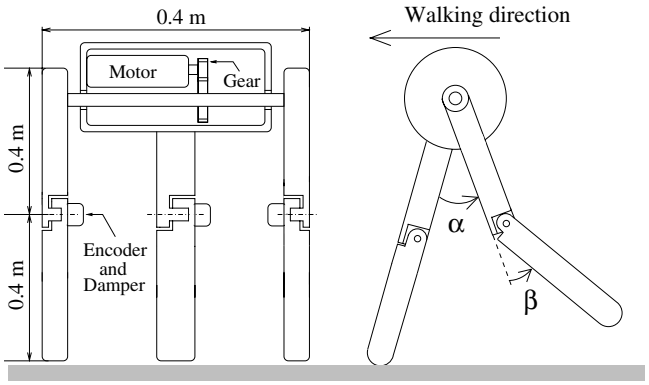

Fig. 17. Outline of biped robot.

the hip and knee is denoted by α and β, respectively, as shown in Figure 15, θ_3 will be estimated by

$$\theta_3 = \frac{1}{2}\alpha + \beta. \tag{10}$$

However, the estimation formula (10) is valid only when both thighs are symmetrical with respect to a vertical line, as shown in Figure 17. The estimation accuracy becomes worse when α is small, as understood from the stick figures in Figure 6a. In the following experiment and numerical simulation, we used eq. (10) to estimate θ_3.

5.2. Modification of the Biped Robot

At the beginning of the experiment, it seemed to be very difficult for the biped robot to walk. After identifying the equivalent values of mass, mass center position, and moment of inertia of each link, including the motor and gears and equivalent viscous damping coefficient at each joint, we simulated the self-excited biped locomotion. As a result, we found that the biped mechanism with these identified parameter values exhibits unstable locomotion with variable step length and is apt to tumble. The manufactured inner and outer legs had different parameter values for each other, and it was found that the difference of mass and the position of mass center between the inner and outer legs are the main causes of unstable locomotion. In addition, the region of initial state conditions, which led the biped to stable locomotion, can be widened by decreasing the difference of mass and mass center position between two legs. Therefore, the difference of the mass and mass offset position was reduced by making many holes in the outer leg frame and by putting an additional mass at the top of each outer leg.

Table 2 shows the measured parameter values of the inner leg and those of the outer legs before and after the improvement. From the numerical simulation using the improved parameter values and measured damping coefficients at joints, it was found that a stable steady walking locomotion can be obtained only when the feedback gain k is near 3.0 Nms/rad. This will be because the residual difference of the link parameter values between the inner and outer legs and the limited accuracy of θ_3 reduce the robustness to the feedback gain. The walking period is changed to about 1.9 s compared with 1.3 s in case of a biped model with a uniform link. The step length is increased to be 0.28 m.

Figure 18 shows the picture of the biped robot after parameter modification. The slender frame, which connects two outer shanks, was added to make their motion synchronize with each other. To maintain the internal force at the knee stopper during the stance phase, an offset angle of 2 degrees was set at the knee stopper. Figure 19 plots the simulated results of $\theta_1, \theta_2, \theta_3$ for the modified parameter values. We note that a stable and steady walking locomotion is possible, although the amplitude of the inner and outer legs is still different in both the support and swing phases because of the residual difference of the parameter values between two legs.

5.3. Experimental Results

To realize a stable biped locomotion in the experiment, it was important to reduce external disturbances and to lead the biped robot into the initial states to converge to a limit cycle motion. The disturbance force from the power supply cable was reduced by introducing light and slender cables, while

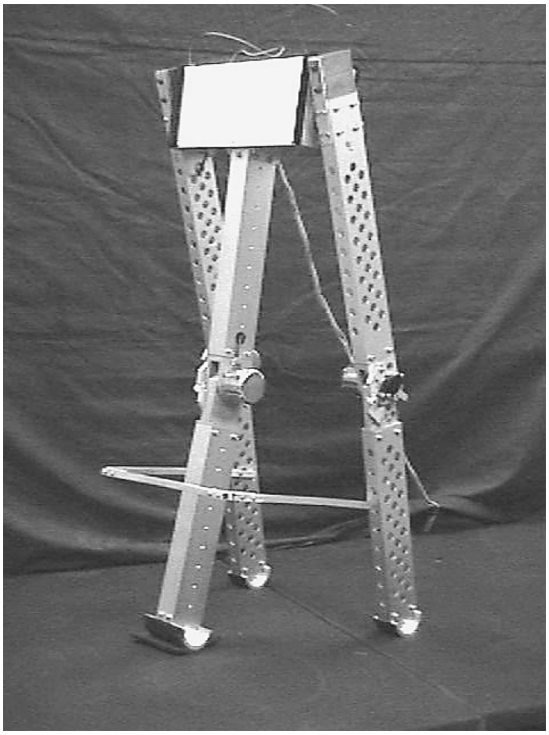

Fig. 18. Biped robot after parameter modification.

Table 2. Parameter Values of a Biped Robot before and after Improvement

	Mass (kg)	Mass Offset (m)	Inertia (kgm^2)
Inner thigh	3.88	0.0784	0.109
Inner shank	1.20	0.192	0.0251
Thigh and shank	5.08	0.200	0.378
Outer thigh	2.64 → 4.26	0.193 → 0.080	0.0791 → 0.1411
Outer shank	1.77 → 1.29	0.190 → 0.195	0.0413 → 0.0266
Thigh and shank	4.41 → 5.55	0.384 → 0.200	0.2895 → 0.4320

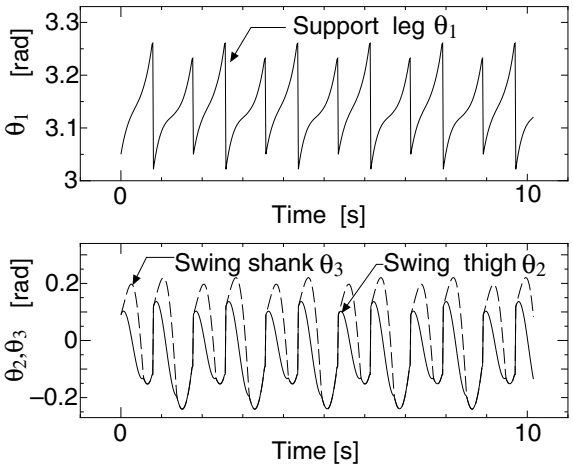

Fig. 19. Simulated results of θ_1, θ_2, and θ_3 for the robot's parameter values.

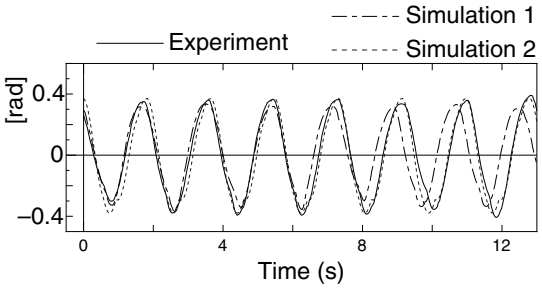

Fig. 20. Comparison of experimental and simulated relative angle of the biped robot.

that from floor was reduced by employing a rigid and flat floor. The adequate initial conditions were learned through a trial-and-error method. As a result, we finally succeeded in realizing the self-excited biped locomotion on a 0.8 degree inclined plane when the feedback gain was about 7 Nm/rad.

The video of the walking locomotion of the biped robot can be observed at http://www.mech.titech.ac.jp/~dycon/ryutaro/Welcome1.html.

Figure 20 comparatively shows the experimental and simulated results of the relative hip angle α. Simulation 1, indicated by a chained line, is the simulated result of the biped robot locomotion on level ground when $k = 3.0$ Nm/rad. To investigate the reason why the biped robot could not walk on the level plane, we compared precisely the simulated and measured angular motion of the support leg before and after the collision with the wooden floor. As a result, we found that the decrease of the measured angular velocity of the support leg from the swing phase is slightly larger than the simulated one based on the conservation laws of momentum and angular momentum. The simulated angular velocity of the support leg after collision agreed with the measured one if we assume that $\dot{\theta}_1^+, \dot{\theta}_2^+, \dot{\theta}_3^+$ are further reduced to $0.94\dot{\theta}_1^+, 0.94\dot{\theta}_2^+, 0.94\dot{\theta}_3^+$ due to a resistive impulse moment at the heel collision. Moreover, we found that the biped model cannot walk on a level floor in the simulation if a 0.94 reduction of these angular velocities is taken into account. Simulation 2, represented by a dotted line, is the calculated result for the floor with a 0.8 degree inclined angle, taking the coefficient of restitution of 0.94 into account. We note that simulation 2 agrees with the experimental result better than simulation 1. The experimental walking period is 1.9 s, walking velocity is 0.29 m/s, and step length is about 0.28 m. The feedback gain k was chosen to be 7.0 N/rad in the experiment because stable walking was hardly recognized at any other values of k. When k was increased, the knee was apt to bend at the beginning of the stance phase. On a level floor, the step length decreased and walking locomotion could not be maintained.

The reason that stable locomotion could not be realized on a level floor is considered as follows: the link parameters of the inner and outer legs could not be sufficiently equalized so that stable walking is possible only in a narrow range of k values. In addition, the loss of kinetic energy in the system at both foot and knee collisions with a 2 degree offset is larger than that of the analytical model. Thus, the dissipated kinetic energy has to be compensated by gravity potential energy because the active input energy cannot be increased by the increase in the feedback gain k.

6. Conclusions

To develop an efficient control method of natural biped locomotion, the self-excitation control of asymmetry stiffness

matrix type was applied to the biped mechanism to generate natural walking locomotion. The theoretical and experimental study are summarized as follows:

1. In a two-DOF swing leg whose thigh and shank are connected by a passive knee joint with and without a knee stopper, the input torque at the hip joint (i.e., feedback from the shank angle) can generate a walking gait of the swing leg and can increase the swing amplitude and its kinetic energy.

2. In a biped model in which two legs are connected serially by a hip motor and each leg has a thigh, shank, and passive knee joint with a knee stopper, we showed numerically that a stable natural walking locomotion can be generated as a limit cycle of the system by applying the self-excitation control of asymmetry stiffness matrix type to the swing leg. The initial state conditions that converge to a steady walking locomotion are wide, and the steady locomotion is robust against the feedback gain if the two legs have the same mechanical parameter values.

3. The period of self-excited biped locomotion depends only on the mechanical parameter values and is hardly influenced by the feedback gain k. By increasing k, the walking velocity increases slightly because of the increase in the step length. However, the efficiency (average walking velocity/average input power) decreases as k increases because the increase in k mainly results in an increase in the height of the swing leg tip.

4. From the simulation for a biped mechanism whose leg is as tall as 0.8 m (similar to a standard adult), the walking period is 1.3 s and walking velocity 0.28 m/s (1.01 km/h) at an average input power of 4 W. Considering that the walking speed is increased due to a foot length of 0.3 m, the calculated natural walking period and velocity seem to be comparable with those of an adult with a 0.8 m leg height.

5. When the mass of the leg is proportional to the square of the leg length, walking velocity is almost constant in a range of leg length from 0.65 m to 0.9 m. Efficiency increases as the leg length decreases. Stable walking can be easily obtained when the shank length is a little larger than the thigh length. The shank length ratio of 0.55 to leg length in human adults is optimal in terms of swing leg clearance and a compromising point between walking velocity and efficiency. A smaller mass ratio of shank to thigh is better in terms of both walking velocity and efficiency.

6. We manufactured a biped robot that has an inner leg and a couple of outer legs. The outer legs are serially connected through a hip motor with one-tenth reduction gears similar to the analytical model. Each leg has a thigh and shank that are connected by a passive joint with a knee stopper. After parameter modification and disturbance reduction, the biped robot could walk on the 0.8 degree inclined plane with a walking period of 1.9 s, step length of 0.28 m, and velocity of 0.29 m/s.

7. Calculated walking locomotion for the biped robot agrees with the experimental one if a reduction factor of 0.94 in the link angular velocities is taken into account at the collision of the leg with the wooden floor.

The self-excited walking could not be realized on a level plane because the actual dissipated energy due to the collision of the leg tip with the floor was larger than the calculated one; it could not sufficiently be compensated by the self-excited control because a stable biped locomotion could not be obtained by a large feedback gain due to the residual difference of parameter values between the inner and outer legs. Realization of self-excited walking on a level plane and self-excited walking of a biped robot with feet are the next goal of our study. More detailed analysis of the limit cycle and some bifurcation phenomena observed near the boundary of one period of stable walking in the self-excited biped system is also our future work.

Appendix A

$$
\begin{aligned}
M_{11} &= I_1 + m_1 a_1^2 + m_2 l_1^2 + m_3 l_1^2 \\
M_{12} &= (m_2 a_2 + m_3 l_2) l_1 \cos(\theta_2 - \theta_1) \\
M_{13} &= m_3 a_3 l_1 \cos(\theta_3 - \theta_1) \\
M_{22} &= I_2 + m_2 a_2^2 + m_3 l_2^2 \\
M_{23} &= m_3 a_3 l_2 \cos(\theta_3 - \theta_2) \\
M_{33} &= I_3 + m_3 a_3^2
\end{aligned} \tag{11}
$$

$$
\begin{aligned}
C_{12} &= -(m_3 a_2 + m_3 l_2) l_1 \sin(\theta_2 - \theta_1) \\
C_{13} &= -m_3 a_3 l_1 \sin(\theta_3 - \theta_1) \\
C_{23} &= m_3 a_3 l_2 \sin(\theta_3 - \theta_2)
\end{aligned} \tag{12}
$$

$$
\begin{aligned}
K_1 &= (m_1 a_1 + m_2 l_1 + m_3 l_1) g \sin\theta_1 \\
K_2 &= (m_2 a_2 + m_3 l_2) g \sin\theta_2 \\
K_3 &= m_3 a_3 g \sin\theta_3
\end{aligned} \tag{13}
$$

Appendix B

$$
\begin{aligned}
f_1(\theta_1, \dot{\theta}_1^-) &= I_1\dot{\theta}_1^- + \{a_1 m_1 v_{1x} + l_1(m_2 v_{2x} + m_3 v_{3x})\} \\
&\quad \cos\theta_1 + \{a_1 m_1 v_{1y} + l_1(m_2 v_{2y} + m_3 v_{3y})\} \sin\theta_1 \\
f_2(\theta_2, \dot{\theta}_2^-) &= I_2\dot{\theta}_2^- + (a_2 m_2 v_{2x} + l_2 m_3 v_{3x}) \cos\theta_2 \\
&\quad + \{a_2 m_2 v_{2y} + l_2 m_2 v_{3y}) \sin\theta_2 \\
f_3(\theta_3, \dot{\theta}_3^-) &= I_3\dot{\theta}_3^- + a_3 m_3 v_{3x} \cos\theta_3 + a_3 m_3 v_{3y} \sin\theta_3,
\end{aligned} \tag{14}
$$

where v_{ix} and v_{iy} are horizontal and vertical velocities of the mass center of the ith link.

Acknowledgment

This research is supported by the grant-in-aid for the COE Research Project of Super Mechano-Systems by the Ministry of Education, Science, Culture and Sport in Japan.

References

Furusho, J., and Masubuchi, M. 1986. Control of a dynamical biped locomotion system for steady walking. *Journal of Dynamic Systems, Measurement, and Control* 108(2):111–118.

Garcia, M., Chatterrjee, A., Riuna, A., and Coleman, M. J. 1998. The simplest walking model: Stability, complexity, and scaling. *ASME Journal of Biomechanical Engineering* 120(2):281–288.

Goswami, A., Espiau, B., and Keramane, A. 1997. Limit cycles in a passive compass gait biped and passivity-mimicking control laws. *Journal of Autonomous Robots* 4(3):273–286.

Goswami, A., Thuilot, B., and Espiau, B. 1998. A study of the passive gait of a compass-like biped robot: Symmetry and chaos. *International Journal of Robotics Research* 17(12):1282–1301.

Hirai, K., Hirose, M., Haikawa, Y., and Takenaka, T. 1998. The development of Honda humanoid robot. *Proceedings of the IEEE International Conference on Robotics and Automation*, Leuven, Belgium, pp. 983–985.

Kajita, S., and Kobayashi, A. 1987. Dynamic walk control of a biped robot with potential energy conserving orbit. *Journal of SICE* 23(3):281–287.

Kato, T., Takanishi, A., Naito, G., and Kato, I. 1981. The realization of the quasi dynamic walking by the biped walking machine. *Proceedings of the International Symposium on Theory and Practice and Manipulators*, ROMANSY, pp. 341–351.

McGeer, T. 1990. Passive dynamic walking. *International Journal of Robotics Research* 9(2):62–81.

Mita, T., Ymagaguchi, T., Kashiwase, T., and Kawase, T. 1984. Realization of a high speed biped using modern control theory. *International Journal of Control* 40(1):107–119.

Miura, H., and Shimoyama, I. 1984. Dynamic walk of a biped. *International Journal of Robotics Research* 3(2):60–74.

Miyazaki, F., and Arimoto, S. 1980. A control theoretic study on dynamical biped locomotion. *Journal of Dynamic Systems, Measurement, and Control* 102(4):233–239.

Ono, K., and Okada, T. 1994a. Self-excited vibratory actuator (1st report: Analysis of two-degree-of-freedom self-excited systems). *Transactions of the JSME(C)* 60(577):92–99 (in Japanese).

Ono, K., and Okada, T. 1994b. Self-excited vibratory actuator (2nd report: Self-excitation of insect wing model). *Transactions of the JSME(C)* 60(579):117–124 (in Japanese).

Ono, K., and Okada, T. 1994c. Self-excited vibratory actuator (3rd report: Biped walking mechanism by self-excitation). *Transactions of the JSME(C)* 60(579):125–132 (in Japanese).

Pratt, J. E., and Pratt, G. A. 1998. Exploiting natural dynamics in the control of a planar bipedal walking robot. *Proceedings of the 36th Annual Allerton Conference on Communication, Control and Computing*.

Sano, A., and Furusho, J., 1990. 3D dynamic walking of biped robot by controlling the angular momentum. *Journal of the SICE* 26(4):459–466.

Spong, M. W. 1999. Passivity based control of the compass gait robot. *IFAC World Congress*, Beijing, China.

Yamaguchi, J., Soga, E., Inoue, S., and Takanishi, A. 1999. Development of a biped humanoid robot-control method of whole body cooperative dynamic biped walking. *Proceedings of the 1999 IEEE International Conference on Robotics and Automation*, pp. 368–374.

Yang, J. S. 1994. A control study of a kneeless biped locomotion system. *Journal of the Franklin Institute (Great Britain)* 331B(2):125–143.